Localization of non-stationary tonal sources through order-based beamforming

K Kottakota, Jérôme Antoni, Quentin Leclere, S Bouley, C Colangeli

Localization of non-stationary tonal sources through order-based beamforming

K. Kottakota [1,2]**, J. Antoni** [2]**, Q. Leclère** [2]**, S. Bouley** [1]**, C. Colangeli** [3]
[1] MicrodB,
28 Chemin du Petit Bois, F-69134, Écully Cedex, France
e-mail: **kalasagarreddi.kottakota@microdb.fr**

[2] Univ Lyon, INSA Lyon, LVA, EA677,
69621 Villeurbanne, France

[3] Siemens Industry Software NV,
Interleuvenlaan 68, 3001 Leuven, Belgium

Abstract
Spectral acoustic imaging is a widely used approach in the automotive industry for sound source localization. However, because the vibroacoustic mechanisms in rotating machines are non-stationary during run-up or run-down, conventional techniques cannot be directly implemented. This necessitates the development of an acoustic imaging method for source localization to deal with non-stationary engine speeds. Order-tracking is a well-known technique to analyze a machine under large speed variation, which has an ability to extract orders, that are proportional to shaft rotational frequency, investigate critical frequencies and tonal components. In this paper, a novel method, coined Order-Based Beamforming (OBBF) is presented. OBBF performs beamforming on extracted orders to localize the sources at various speeds during a run-up or run-down. The proposed method is evaluated through both simulated and experimental data. The key outcome of this work is to show the automotive industry a way to perform localization at non-stationary operating conditions.

1 Introduction

Transportation noise and air pollution have emerged as widespread issues, causing long-term and negative impacts on human health such as respiratory infections, severe annoyances, sleep disruptions, and cognitive impairment in children [1, 2]. As a result, authorities are constantly enacting stringent regulations in an effort to improve human health while also achieving a zero-emission footprint through improved fuel economy, prompting automakers to shift their focus to Battery Electric Vehicles (BEV) and hybrid vehicles with downsized engines. In 2011, Goetchius [3] published an assessment of the contribution of noise sources in BEV's to the overall effort. The absence of combustion engine drastically alters the acoustic signature, making component noises noticeable and even predominant, resulting in an unappealing sound quality. Therefore, one of the major challenges is to control the acoustic signature of the vehicle components. The first step of the acoustic refinement is localization of potential noise sources and their contribution to the overall sound pressure level. Thus, the automotive industry invests great deal of time and effort to gain high level of competence in understanding the noise and vibration issues, making experimentation unavoidable.

Rotating machines, such as Internal Combustion Engine (ICE) or a gear-box are often tested in a run-up / run-down mode for Noise, Vibration & Harshness (NVH) diagnosis. The majority of them feature orders that are time varying phasors which rotate with an instantaneous frequency linked to the main shaft rotational speed [4, 5]. Order Tracking (OT) is a measurement technique capable of investigating the orders from such dynamic rotating machinery operating in the modes described above. Unlike spectral-domain functions, which use frequency as the independent variable, OT examines response signals as a function

of shaft rotational speed. There are two types of OT techniques: Fourier-based [6] and time-domain [7]. Vold-Kalman Filter (VKF) tracking [7] and baseband demodulation [8] are OT techniques implemented in time domain that use the instantaneous speed of rotation as *a priori* information. The main outputs of OT that facilitate NVH diagnosis are colormap plots which depicts orders and resonances present in the system. They have time or revolutions per minute (rpm) as x-axis, frequency or orders as y-axis, and amplitude as the color-axis. When using order analysis to investigate noise sources, one may only determine resonances, or a tonal / broadband component existing in a certain frequency range and perhaps make inferences about the impacts of various frequencies [9]. On the other hand, combining order analysis with acoustic imaging, produce source maps that may be used to localize dominant sources within the desired frequency range.

Acoustic imaging based on pressure measurements from a microphone array have been proven to be an effective tool for localizing and quantifying noise sources since the 70's and have been extensively adapted for the use in the automotive industry. Over the past decades, the increasing capability of computers and data acquisition systems have spurred the rapid development of several advanced array techniques known as beamforming-type and inverse methods [10], robustly operating in the spectral domain. Among them, the most widespread post-processing algorithm is conventional beamforming. The measured responses during a run-up / down are non-stationary, where the signal is amplitude and frequency modulated. However, because the generated vibroacoustic phenomenon is a function of shaft rotational speed rather than absolute frequency only, the conventional techniques developed for stationary condition cannot be directly implemented. Nonetheless, run-up or down can be analyzed to some extent by Short-Time Fourier Transform (STFT). The fundamental challenge with STFT is the bandwidth-time constraint imposed by the Heisenberg uncertainty principle, which means that a short duration of STFT will limit frequency resolution. The other limitation is the smearing effect, in which the energy associated with each frequency leaks into the adjacent frequency bins. Because the microphone signals are non-stationary, the spectrum of the signal is not constant over the time block, which distributes the contribution of orders on multiple frequency bins. As a result, in order to simulate the approximate stationary assumption, the machines are subjected to low slew rates to define quasi-stationary assumption for each block. On the contrary, machines where high slew rates are unavoidable or that have close / crossing orders [11, 12], increase the complexity of the analysis. For nominal rpm, STFT requires a smaller snapshot block size to estimate its corresponding response, which affects both spectral resolution and smearing. Moreover, when analyzing close tonal components, the effects are exacerbated because, poor resolution obscures the ability to identify individual tones and their sources. This calls for the development of stand-alone acoustic imaging techniques for non-stationary source localization, where phased microphone array processing is performed on an extracted order to localize sound sources. In this manuscript, time-domain OT method baseband demodulation, which is independent of Fourier and Heisenberg restrictions, is used to extract orders.

Few authors discussed localization of sound sources on orders. Among them, Hald discussed the implementation of Near-field Acoustic Holography (NAH) with orders [13]. He pioneered the Non-Stationary Spatial Transformation of Sound Field (NS-STSF) based on Time-Domain Holography (TDH) [14] to analyse non-stationary sources. The approach generates time-based quantities such as sound pressure, intensity, or power that may be processed by an order-based filter to determine the location of order-based sound sources. However, his method is confined to planar sources and can only compute acoustic quantities on a plane parallel to the array plane. Subsequent research by the scientific community has yielded several NAH techniques [15] for studying non-stationary sources, but they are always constrained by the shape of the object. Using the cyclostationarity property of signals acquired from an engine operating in stationary condition, Lafon *et al.* [16] described a new acoustical term, cyclic sound intensity, which allowed the construction of radiation movies in angle-frequency domain during an average engine cycle. In [17, 18], acoustic holography and continuous-scan beamforming are used to localize harmonic and broadband sources in a turbofan measured at quasi-stationary conditions. The harmonic and broadband components of the total measured response were separated by a time-domain VKF. In an investigation to study the distribution of sound sources in an standalone Counter-Rotating Open Rotor (CROR) aerospace engine, Horvath *et al.* [19, 20] applied conventional beamforming, to address the sound sources associated with the Blade Passing Frequencies (BPF's) and its harmonics as well as the interaction tones of the front and rear rotors. As the spectral peaks are associated with the rotational frequency, the results were expressed in shaft orders rather than Hertz. In general, they separated the sources associated with tonal and broadband components, which aided them understand the

noise generation mechanism. Fenyvesi *et al.* [9] further investigated the installation effects of pylon to the CROR acoustic radiation and defined a flowchart to sort the sound sources into more specific groups by combining order analysis with beamforming maps. The shaft order tones, rotating coherent sound sources, and blade-wake interaction tones might appear in BPF's frequency bins, making sound source separation cumbersome. As a result, using a combination of beamforming maps and order spectrum peaks, they categorised the sources inside the bins. Around the same time, Fenyvesi *et al.* [21] used order analysis, beamforming with Proper Orthogonal Decomposition (POD) to interpret beamforming maps that can contain sidelobes as well as rotating coherent sound sources of the CROR. Beamforming produces a vast frequency bin data collection, making analysis time consuming and difficult. For this, they employed POD methods like Principal Component Analysis with beamforming output. They also demonstrated that this technique can rank the shaft order sound sources. Although the analysis include shaft orders in above literature study, it is limited to stationary condition. In 2020, Le Magueresse *et al.* [22] studied the acoustic radiation of an electric motor from the recordings obtained during a run-up operating condition. In this case, Bayesian focusing is applied to a Cross-Spectral Matrix (CSM) computed for each snapshot for source localization and the measurements were performed at low slew rates to reduce the effect of smearing.

According to the above-mentioned literature review, it appears preferable to analyze rotating machinery with orders under non-stationary operating conditions. All authors aimed to solve a specific problem by employing a certain method. None has developed a theoretical framework and a unified order-based approach for dealing the non-stationary regime that accounts for all of the aforementioned drawbacks. So, as a stepping stone towards developing order-based array processing techniques, this paper introduces Order-Based Beamforming (OBBF), a novel technique in which beamforming is performed on an order. It is also reminded that the interest is to localize the tonal sources and the proposed method wouldn't apply to characterize broadband noise.

The following is a breakdown of the paper's structure: section 2 provides a brief overview of the baseband demodulation order tracking technique. In section 3, direct and inverse formulation of proposed approach i.e. OBBF is introduced. Then section 4, the approach is validated with numerical simulations as well compared with conventional beamforming results. An industrial case study conducted on an electric motor test rig at Siemens, Leuven is presented in section 5 and conclusions are drawn in section 6.

2 Baseband demodulation order tracking technique

The concept of baseband demodulation takes root from communication systems. This is a simple and elegant technique that can been adapted to extract orders. In telecommunications, baseband is defined as a frequency range prior to the modulation. In other words, baseband signal is a lowpass signal with spectral components that are close to zero. On the contrary, passband refers to modulated signal. The overall purpose of demodulation is to use the phasor to recover the complex envelop from the passband signal, which is similar to the other order tracking techniques.

2.1 The structure of orders

Let consider a point source at position $\mathbf{r}_s$. The time evolution function of the emitted signal from the point source is defined as

$$x_s(t) = \sum_{p \in \mathcal{P}} x_{p,s}(t), \tag{1}$$

where $\mathcal{P}$ is the discrete set of orders, $x_{p,s}(t) = A_{xp,s}(t)\mathrm{e}^{\mathrm{j}p\theta(t)}$ is the signal belonging to order p contained in $x_s(t)$ and is defined as an "order" in the engineering community, $A_{xp,s}(t) \in \mathbb{C}$ is the slowly varying complex envelop of order p and $\theta(t) = \int_0^t \omega(u)\mathrm{d}u$ the instantaneous phase of reference with $\omega(u)$ the instantaneous angular frequency.

According to acoustic propagation, in a quiescent medium, under free-field conditions, the pressure field observed at $\mathbf{r}$, produced by $x_s(t)$ is

$$y(t) = h_s(t) * x_s(t), \tag{2}$$

where the symbol * denotes convolution in time, $h_s(t) = H_s\delta\left(t - t_s\right)$ is the Green's function, $t_s = \|\mathbf{r} - \mathbf{r}_s\|/c_0$, c_0 is the speed of sound, δ denotes the Dirac delta function and $H_s = 1/\|\mathbf{r} - \mathbf{r}_s\|$ is the attenuation in acoustic propagation.

In a real case, the total acoustic response $y(t)$ measured at a sensor from a rotating machinery also contains other components, hereafter referred to as noise $\eta(t)$, such that

$$y(t) = \sum_{p\in\mathcal{P}} y_p(t) + \eta(t), \tag{3}$$

where $y_p(t) = h_s(t) * x_{p,s}(t)$.

2.2 The formulation of baseband demodulation order tracking

The aim of this part is to extract $y_p(t)$ from $y(t)$. This is done by baseband demodulation order tracking. For continuous signals, the baseband demodulation order tracking is mathematically described as

$$A_{yp}(t) = g(t) * \left(y(t)\mathrm{e}^{-\mathrm{j}p\theta(t)}\right), \tag{4}$$

where the symbol * denotes convolution in time and $g(t)$ is the impulse response of a low-pass filter.

The measured signal $y(t)$ is multiplied with the conjugate of the complex phasor of the order of interest and accordingly convolved with a lowpass filter to remove the nuisance component containing the non-tracked orders and noise. A Savitzky–Golay lowpass filter is applied in this paper.

Therefore, $y_p(t)$ of order p contained in $y(t)$ is written as

$$y_p(t) = A_{yp}(t)\mathrm{e}^{\mathrm{j}p\theta(t)}. \tag{5}$$

3 Order-based beamforming

This section introduces the signal processing paradigm of OBBF, that establishes forward and inverse relationships between the input and output of a linear time-invariant system excited by an order. The proposed method is fully original, more than a simple application of conventional beamforming to order-tracked orders, based on the inversion of the operator that maps the source orders to the microphone orders. In this method, orders are extracted first from the time signals of the microphone array and then they are next back-propagated towards the calculation plane for the source reconstruction. Moreover, beamforming orders is computationally more efficient than order tracking the output of Time-Domain Beamforming (TBD) [23] because the latter requires all potential sources on the source grid to be order-tracked, the former only requires response signals observed at the array to be order-tracked. In this way, acoustic engineers benefit improved tracking of order envelops compared to the traditional techniques.

Consider a source grid with I calculation points positioned at $\mathbf{r}_i(i \in [1 \cdots I])$ that samples the scanned area and an array of M microphones positioned at $\mathbf{r}_m(m \in [1 \cdots M])$ which samples the sound field. Lets denote $y_m(t)$ as the pressure signal observed at a microphone m, produced by $x_s(t)$ located at $\mathbf{r}_s$. Beamforming of phased microphone array measurements is a sound source localization technique in which pressure signals $\{y_m(t)\}(m \in [1 \cdots M])$ are focused at all possible positions of calculation points $\mathbf{r}_i(i \in [1 \cdots I])$ in a defined source grid, assuming $\mathbf{r}_s$ in the set $\{\mathbf{r}_1, \cdots \mathbf{r}_I\}$. It should be noted that this assumption is just to simplify the exposition; in general, the exact source position could just as well depend on time t. Denote

$y_{p,m}(t)$ to be the order signal tracked in $y_m(t)$. It should be noted at this juncture that the method's overall application on a real-world problem is divided into two parts: a) OT of $\{y_m(t)\}$ and b) OBBF, considering a single order $\{y_{p,m}(t)\}$, order tracked in $\{y_m(t)\}$. However, OBBF employs advanced envelop of order of interest instead of the observed microphone signals during its implementation.

3.1 Direct problem

The aim of the direct problem is to relate the envelops at microphone $A_{yp,m}(t)$ to $A_{xp,s}(t)$ in a way that allows the design of a linear inverse problem. Consider the acoustic propagation of a signal say $x_{p,s}(t)$, a special case of an excitation of the "monocomponent" form with $\theta_p(t)$ the instantaneous phase, emitted from a point source at $\mathbf{r}_s$ to an array composed of M microphones in the order domain is

$$x_{p,s}(t) = A_{xp,s}(t)\mathrm{e}^{\mathrm{j}\theta_p(t)}. \tag{6}$$

Let us now investigate the "order" response $y_{p,m}(t)$ to $x_{p,s}(t)$, as recorded by microphone m, when it passes through the linear-time invariant system as described by Eq. (2).

Consider the general case where the impulse response $h_{sm}(t)$ is proportional to a pure delay, i.e. $h_{sm}(t) = H_{sm}\delta(t - t_{sm})$ with $t_{sm} = \|\mathbf{r}_m - \mathbf{r}_s\|/c_0$ and $\mathbf{r}_m$ is the position of microphone m.

The pressure recorded by microphone m is

$$y_{p,m}(t) = H_{sm}A_{xp,s}(t - t_{sm})\mathrm{e}^{\mathrm{j}\theta_p(t-t_{sm})}. \tag{7}$$

In order to obtain a relationship between $A_{yp,m}(t)$ and $A_{xp,s}(t)$, let $t_{sm} = t_0^s + \tau_{sm}$ with t_0^s a global propagation time (see subsubsection 3.2.1) between the point source and microphones. Then the advanced signal is

$$\begin{aligned} y_{p,m}(t + t_0^s) &= H_{sm}A_{xp,s}(t - \tau_{sm})\mathrm{e}^{\mathrm{j}\theta_p(t-\tau_{sm})} \\ &\simeq H_{sm}\mathrm{e}^{-\mathrm{j}\tau_{sm}\theta'_p(t)}A_{xp,s}(t - \tau_{sm})\mathrm{e}^{\mathrm{j}\theta_p(t)} \quad (8) \\ &= A^{t_0^s}_{yp,m}(t)\mathrm{e}^{\mathrm{j}\theta_p(t)}, \quad (9) \end{aligned}$$

where $A^{t_0^s}_{yp,m}(t) = \mathrm{e}^{\mathrm{j}t_0^s\theta'_p(t)}H_{sm}(f_p(t))A_{xp,s}(t-\tau_{sm})$ is the advance complex envelop of order signal $y_{p,m}(t+t_0^s)$, $H_{sm}(f_p(t)) = H_{sm}\exp(-j2\pi f_p(t)t_{sm})$ is the transfer function and $f_p(t) = \theta'_p(t)/2\pi$.

Employing a 1^{st} order Taylor's expansion for $A_{xp,s}(t - \tau_{sm})$ leads to

$$A^{t_0^s}_{yp,m}(t) \simeq \mathrm{e}^{\mathrm{j}t_0^s\theta'_p(t)}H_{sm}(f_p(t))\left(A_{xp,s}(t) - \tau_{sm}A'_{xp,s}(t)\right). \tag{10}$$

With $\mathbf{A}^{t_0^s}_{yp}(t)$ the vector that collects the advanced envelopes of the M microphones, transfer function $H_{sm}(f_p) = H_{sm}\exp(-\mathrm{j}2\pi f_p t_{sm})$ and with $\mathbf{h}^s_1(t) = \mathrm{e}^{\mathrm{j}t_0^s\theta'_p(t)}[H_{s1}(f_p(t)), \cdots, H_{sM}(f_p(t))]^{\mathrm{T}}$ and $\mathbf{h}^s_2(t) = \mathrm{e}^{\mathrm{j}t_0^s\theta'_p(t)}[-\tau_{s1}H_{s1}(f_p(t)), \cdots, -\tau_{sM}H_{sM}(f_p(t))]^{\mathrm{T}}$, the single-input-multiple-output relationship becomes

$$\mathbf{A}^{t_0^s}_{yp}(t) \simeq \mathbf{h}^s_1(t)A_{xp,s}(t) + \mathbf{h}^s_2(t)A'_{xp,s}(t). \tag{11}$$

Given the knowledge of the transfer function $H_{sm}(f_p)$, the angular function $\theta_p(t)$ and the observation $\mathbf{A}^{t_0^s}_{yp}(t)$, it is thus possible to recover $A_{xp,s}(t)$ by solving a linear inverse problem. There are several approaches to do this. One is to recover $A_{xp,s}(t)$ and $A'_{xp,s}(t)$ together via matrix inversion. Another one is to consider the formulation of a discrete filter.

3.2 Beamforming on orders

The following details the inverse operator for reconstructing the source spatial distribution from the orders tracked from the microphone observed responses. As mentioned above, this section solves the inverse problem with two algorithms, an algorithm based on the matrix inversion of Eq. (11) and a recursive formulation based on the construction of a discrete filter. In a nutshell, the algorithms describe the construction of an equation to recover source envelop, that is used to try all possible calculation positions $\mathbf{r}_i (i \in [1 \cdots I])$, assuming that $\mathbf{r}_s$ lies in $\{\mathbf{r}_1, \cdots \mathbf{r}_I\}$.

3.2.1 Algorithm 1: Matrix inversion based OBBF

Consider beamformer response $A_{xp,i}(t)$ for any position of calculation point $\mathbf{r}_i$ on the source grid. Then based on approximation Eq. (11), a solution to recover $A_{xp,i}(t)$ with matrix inversion is

$$\begin{pmatrix} A_{xp,i}(t) \\ A'_{xp,i}(t) \end{pmatrix} = \mathbf{H}^{+}(t)\mathbf{A}_{yp}^{t_0^i}(t), \tag{12}$$

where $\mathbf{H}^{+} = (\mathbf{H}^{\mathrm{H}}\mathbf{H})^{-1}\mathbf{H}^{\mathrm{H}}$ is the pseudoinverse of matrix $\mathbf{H} = [\mathrm{h}_1^i \ \mathbf{h}_2^i]$. The estimated $\hat{A}_{xp,i}(t)$ reads

$$\hat{A}_{xp,i}(t) = \frac{\left(\|\mathbf{h}_2^i(t)\|^2 \mathbf{h}_1^i(t)^{\mathrm{H}} - \mathbf{h}_1^i(t)^{\mathrm{H}}\mathbf{h}_2^i(t)\mathbf{h}_2^i(t)^{\mathrm{H}}\right) \mathrm{A}_{yp}^{t_0^i}(t)}{\|\mathbf{h}_1^i(t)\|^2\|\mathbf{h}_2^i(t)\|^2 - |\mathbf{h}_2^i(t)^{\mathrm{H}}\mathbf{h}_1^i(t)|^2}. \tag{13}$$

Accordingly, if the array is focused on the correct source position i.e. $\mathbf{r}_i = \mathbf{r}_s$, then $\hat{A}_{xp,i}(t) \simeq A_{xp,s}(t)$ and it should also be noted that in Eq. (12), $A'_{xp,i}(t)$ acts as an intermediate variable to properly recover $A_{xp,i}(t)$.

The numerical precision of the above solution will be driven by the denominator. Some insight can be gained under the far-field assumption. Then $H_{im}(f_p) = \exp(-\mathrm{j}2\pi f_p t_{im})/R$, with R a propagation distance between the calculation point and far-field array and constant $\forall m$, $\|\mathbf{h}_1^i\|^2 = M/R^2$, $\|\mathbf{h}_2^i\|^2 = \sum_m \tau_{im}^2/R^2$, and $|\mathbf{h}_2^{i^{\mathrm{H}}}\mathbf{h}_1|^2 = |\sum_m \tau_{im}|^2/R^4$. Therefore, the denominator is

$$\begin{aligned} \|\mathbf{h}_1^i\|^2\|\mathbf{h}_2^i\|^2 - |\mathbf{h}_2^{i^{\mathrm{H}}}\mathbf{h}_1^i|^2 &= (M\sum_m \tau_{im}^2 - |\sum_m \tau_{im}|^2)/R^4, \\ &= \frac{M^2}{R^4}\left(\overline{\tau^2} - \overline{\tau}^2\right), \end{aligned} \tag{14}$$

with $\overline{\tau}$ and $\overline{\tau^2}$ the averages of τ and τ^2, respectively. The latter is maximized when $\overline{\tau} = \sum_{m=1}^{M} \tau_{im}/M = 0$. This indicates that t_0^i should be chosen accordingly, for instance by defining it as the propagation time of a point source located at the center of the array of microphones. In the general case (not necessarily a far-field), the denominator is similarly given by

$$\|\mathbf{h}_1^i\|^2\|\mathbf{h}_2^i\|^2 - |\mathbf{h}_2^{i^{\mathrm{H}}}\mathbf{h}_1^i|^2 = (\sum_{m=1}^{M} |H_{im}|^2)^2 \left(\overline{\tau^2}_{H,i} - \overline{\tau}_{H,i}^2\right), \tag{15}$$

where

$$\overline{\tau}_{H,i} = \frac{\sum_{m=1}^{M} \tau_{im}|H_{im}|^2}{\sum_{m=1}^{M} |H_{im}|^2} \tag{16}$$

and

$$\overline{\tau^2}_{H,i} = \frac{\sum_{m=1}^{M} \tau_{im}^2|H_{im}|^2}{\sum_{m=1}^{M} |H_{im}|^2} \tag{17}$$

are weighed averages. Here again, the Eq. (15) is maximized when $\overline{\tau}_{H,i} = 0$.

An important remark is that if $\tau_{im} (m \in [1 \cdots M])$ is constructed such that $\overline{\tau}_{H,i} = 0$, this is equivalent to having $\mathbf{h}_1^i(t)^{\mathrm{H}}\mathbf{h}_2^i(t) = 0$. Therefore

$$\hat{A}_{xp,i}(t) = \frac{\mathbf{h}_1^i(t)^{\mathrm{H}} \mathbf{A}_{yp}^{t_0^i}(t)}{\|\mathbf{h}_1^i(t)\|^2}, \tag{18}$$

which is recognized analogous to conventional beamforming on the advanced complex envelope with the steering vector tuned at frequency $f_p(t) = \theta_p'(t)/2\pi$ (see subsection 3.3).

The selection of t_0^i can be performed by considering the definition $t_{im} = t_0^i + \tau_{im}$. And a general condition for $\overline{\tau}_{H,i} = 0$,

$$t_0^i = \frac{\sum_{m=1}^{M} t_{im}|H_{im}|^2}{\sum_{m=1}^{M} |H_{im}|^2}. \tag{19}$$

3.2.2 Algorithm 2: Recursive OBBF

The algorithm outlines the construction of a recursive discrete filter to recover the envelop $A_{xp,i}(t)$ for any position of calculation point $\mathbf{r}_i$, by employing a finite difference scheme to $A'_{xp,i}(t)$ in Eq. (11). Therefore, the procedure starts with applying a first order backward finite difference scheme for $A'_{xp,i}(t) \simeq \left(A_{xp,i}(t) - A_{xp,i}(t-\Delta t)\right)/\Delta t$ and solving for $A_{xp,i}(t)$ yields

$$A_{xp,i}(t) = \left(\frac{\mathbf{h}_2^i(t)}{\Delta t \mathbf{h}_1^i(t) + \mathbf{h}_2^i(t)}\right) A_{xp,i}(t-\Delta t) + \left(\frac{\Delta t}{\Delta t \mathbf{h}_1^i(t) + \mathbf{h}_2^i(t)}\right) \mathbf{A}_{yp}^{t_0^i}(t), \tag{20}$$

Now, denoting $A_{xp,i}[n] = A_{xp,i}(n\Delta t)$, $\mathbf{A}_{yp}^{t_0^i}[n] = \mathbf{A}_{yp}^{t_0^i}(n\Delta t)$, the Multiple Input Single Output (MISO) case leads to a recursive filter of form

$$A_{xp,i}[n] = \left(\Delta t \mathbf{h}_1^i[n] + \mathbf{h}_2^i[n]\right)^{+} \left(\mathbf{h}_2^i[n] A_{xp,i}[n-1] + \Delta t \mathbf{A}_{yp,i}^{t_0^i}[n]\right). \tag{21}$$

where $\mathbf{h}_1^i[n] = \mathbf{h}_1^i(n\Delta t)$, $\mathbf{h}_2^i[n] = \mathbf{h}_2^i(n\Delta t)$ for $n = 1, 2, ...N$ and $^+$ denotes pseudoinverse of the matrix and $\Delta t = \mathrm{d}t$ the time sample.

Equation (21) links the microphone orders to the source orders to perform localization. Similarly, higher order schemes can be easily conceived by following the same lines with higher-order Taylor expansion.

Equation (21) is causal in nature, which demands an initial value. A simple way to initialize for first sample (i.e. $n = 0$) of the recursive filter is to use a zero-th order approximation to find $A_{xp,i}[0]$,

$$A_{xp,i}[0] = \mathbf{h}_1^{i^+}[0] \mathbf{A}_{yp}^{t_0^i}[0]. \tag{22}$$

For the discrete filter to be stable, one must have

$$\left|\left(\Delta t \mathbf{h}_1^i[n] + \mathbf{h}_2^i[n]\right)^{+} \mathbf{h}_2^i[n]\right| < 1. \tag{23}$$

Setting $\mathbf{u} = \Delta t \mathbf{h}_1^i[n] + \mathbf{h}_2^i[n]$ and $\mathbf{v} = \mathbf{h}_2^i[n]$, the condition reads

$$\frac{|\mathbf{u}^{\mathrm{H}}\mathbf{v}|}{\|\mathbf{u}\|^2} < 1 \Longleftrightarrow |\mathbf{u}^{\mathrm{H}}\mathbf{v}| < \|\mathbf{u}\|^2. \tag{24}$$

Using the explicit expressions of $\mathbf{h}_1^i[n]$ and $\mathbf{h}_2^i[n]$, this becomes

$$\left|\sum_{m=1}^{M} \tau_{im}(\Delta t - \tau_{im})|H_{im}|^2\right| < \sum_{m=1}^{M} (\Delta t - \tau_{im})^2 |H_{im}|^2. \tag{25}$$

The first interesting condition for the filter to be always stable is when $\overline{\tau}_{H,i} = \sum_{m=1}^{M} \tau_{im}|H_{im}|^2 = 0$ which corresponds to as given in Eq. (19); then the Eq. (25) becomes $0 < \Delta t^2 \sum_{m=1}^{M} |H_{im}|^2$, which is always satisfied. This condition is the same that was found for the matrix inversion solution in the previous subsection. Although it is a sufficient condition, it is not the best one. However, the second condition devised from Eq. (25), $\overline{\tau}_{H,i} < \Delta t$ provides a better solution. A case that satisfies the second condition is by considering $t_0^i = \max[t_{i1}, \cdots, t_{iM}]$, which makes the filter more stable to perform recursive OBBF.

As beamforming is performed considering each single calculation point on the grid, ideally demands t_0^i to be chosen I times during the implementation i.e. advancing $y_{p,m}(t)$ and demodulating $y_{p,m}(t+t_0^i)$ to extract the advanced envelop $A_{y,m}^{t_0^i}(t)$. For the sake of simplicity, i.e. to avoid the above-mentioned implementation issues , t_0^i can be fixed for all the calculation points by chosing it as $\max(\mathbf{r}_{im}/c_0)(i \in [1 \cdots I]; m \in [1 \cdots M])$, where $\mathbf{r}_{im}$ is the propagation distance from m^{th} microphone to i^{th} calculation point.

3.3 Conventional beamforming (CBF)

This section describes the application of the classical technique CBF, which is commonly used to analyze non-stationary regimes, as well as show its structural resemblance to OBBF in Eq. (18). As mentioned in the section 1, STFT is used to investigate conditions such as run-up / down. Then STFT of signal $y_m(t)$ is defined as

$$Y_m(t,f) = \int_{-\infty}^{+\infty} w(t-u) y_m(u) \mathrm{e}^{-\mathrm{j}2\pi f u} \mathrm{d}u, \tag{26}$$

where $w(u)$ is a data window function and similarly $X_i(t,f)$ stands for the STFT of $x_i(t)$ in Eq. (1).

CBF assumes that $X_i(t,f)$ and $Y_m(t,f)$ are related as

$$Y_m(t,f) \simeq H_{im}(f) X_i(t,f), \tag{27}$$

It is also inferred that, for a more exact relationship of CBF would be $Y_m(t,f) \simeq H_{im}(f) X_i(t-\tau_{im}, f)$ (although never used in practice), in analogy to Eq. (8).

With $\mathbf{Y}(t,f) = [Y_1(t,f) ... Y_M(t,f)]^{\mathrm{T}} \in \mathbb{C}^M$ the vector that collects the pressures at frequency f and steering vector $\mathbf{h}_i = [H_{i1}(f) ... H_{iM}(f)]^{\mathrm{T}}$, an estimate returned by conventional beamforming is expressed as

$$\hat{X}_i(t,f) = \frac{\mathbf{h}_i(f)^{\mathrm{H}} \mathbf{Y}(t,f)}{\|\mathbf{h}_i(f)\|^2}. \tag{28}$$

Therefore, from Eq. (28), it is evident that at the end CBF is analogous to Eq. (18), where the STFT is used instead of orders. However, STFT suffers from the Heisenberg principle, in contrast to OBBF.

4 Numerical simulation

In this section, the feasibility of localizing and quantifying the non-stationary sources using order-based beamforming is examined through a numerical simulation. Both the algorithms matrix-inversion and recursive OBBF are tested. One of the scenarios occurring in variety of rotating machines [11, 12] i.e. close orders is carefully designed in an attempt to demonstrate the capability of order-based beamforming to track order related sources. The results of OBBF are compared to conventional beamforming, which is detailed in Ref. [24] and presented in subsection 3.3.

4.1 Simulation configuration

A 1D time-domain run up simulation of high slew rate is designed to demonstrate the capability of OBBF in addressing the drawbacks discussed in Sec.1. The simulation scenario here deals with sources of close orders. As shown in Fig. 1a, the simulation model consists of three spatially separated point sources, namely s_1, s_2 and s_3 placed on a source-grid and with a linear microphone array at a distance of $0.4\,\mathrm{m}$ from it. This part deals with the localization and reconstruction of non-stationary point sources radiating in free-field towards a linear array with the reference frequency linearly increasing from $10\,\mathrm{Hz}$ to $200\,\mathrm{Hz}$, amplitude modulation with exponential increasing and decreasing envelop tracks described in Table 1; spanning a total time $T = 5\,\mathrm{s}$ and sampling frequency of $f_s = 24\,576\,\mathrm{Hz}$. The three sources are explained in detail in Table 1. Two of the sources s_2 and s_3 represent close orders in the system. The response observed at the linear microphone array involves three orders, and random noise is added so that Signal-to-Noise Ratio (SNR) $5\,\mathrm{dB}$ for each microphone, as shown in the time-frequency map in Fig. 1b. The simulation described here is solved for the localization of the source associated with order 24.85. To solve the inverse problem, both conventional beamforming and order-based beamforming are used.

Table 1: Point sources description.

Source	Order	$f_{\min}$ [Hz]	$f_{\max}$ [Hz]	Coordinate x [m]	Complex envelop	Source peak amplitude
s_1	1	10	200	-0.4	$100\mathrm{e}^{-\lvert t-2\rvert}$	100
s_2	24.85	248.5	4970	0.6	$150\mathrm{e}^{-\lvert t-2.5\rvert}$	150
s_3	25	250	5000	0	$120\mathrm{e}^{-\lvert t-4\rvert}$	120

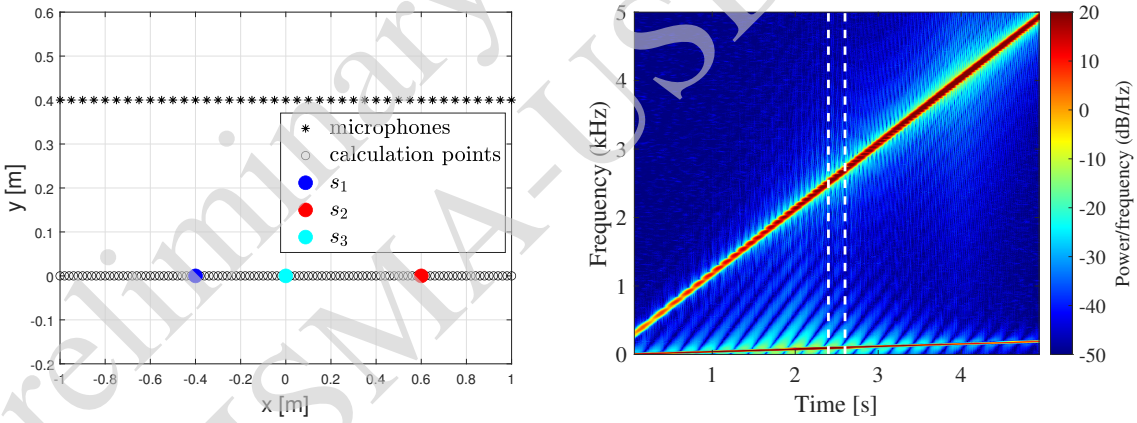

(a) (b)

Figure 1: Schematic of a simulation model: (a) the simulation model with three point sources and a linear array and (b) the spectrogram of an array microphone with order 1 and close orders 24.85 and 25; vertical dashed white lines represents the selected time block of $0.2\,\mathrm{s}$ for Fourier Transform.

4.2 Solution with conventional beamforming

CBF described in subsection 3.3 applied in this part to investigate the simulation model that contains close orders. The aim of the problem is to localize the source s_2 associated with the order 24.85. Figure 2a depicts the spectrum of an array microphone with $df = 5\,\mathrm{Hz}$ corresponding to the selected time block of $0.2\,\mathrm{s}$ spanning $2.4\,\mathrm{s}$ to $2.6\,\mathrm{s}$ as shown in Fig. 1b. The spectrum ranging from $2500\,\mathrm{Hz}$ to $2725\,\mathrm{Hz}$ corresponds to the orders 24.85 and 25. CBF calculated for a selected frequency $2615\,\mathrm{Hz}$ as shown in Fig. 2b, demonstrates the presence of two sources s_2 and s_3 in contrary to the aim of the problem, i.e. to localize the source s_2 associated to order 24.85. This is because of the effect of smearing discussed in section 1, where the

energy corresponding to the frequency 2615 Hz is shared between the sources s_2 and s_3. Therefore, it can be inferred that CBF fails to track the sources associated with individual orders in a system composed of close orders. Furthermore, Fig. 2b also illustrates the disparity between the actual and reconstructed source amplitude caused due to smearing, demonstrates the ineffectiveness of CBF when attempting to quantify a non-stationary source.

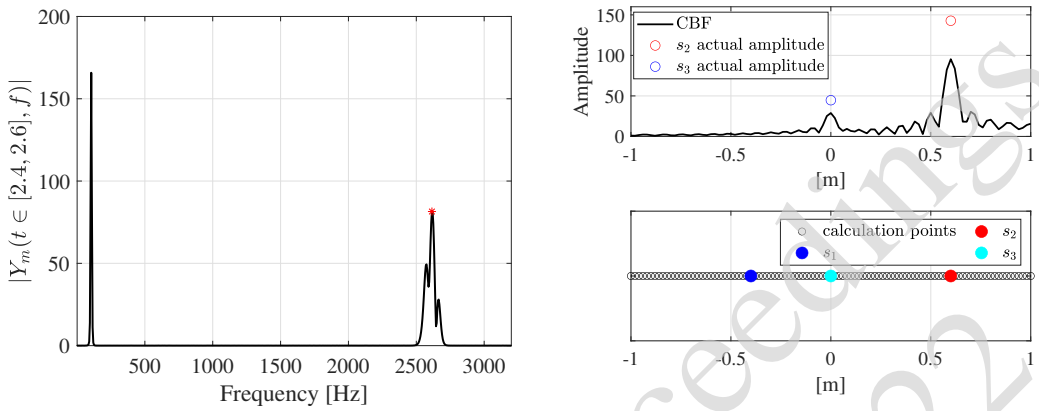

(a) (b)

Figure 2: Solution with conventional beamforming: (a) spectrum of an array microphone with $df = 5$ Hz; red star denotes 2615 Hz and (b) CBF source map at 2615 Hz.

4.3 Solution with order-based beamforming

In this part, the simulation model is solved by OBBF. The process begins with the extraction of order of interest, i.e. 24.85, which is accomplished through baseband demodulation order tracking discussed in Sec. 2. Both the inverse schemes are applied to generate a source map and reconstruct $\hat{A}_{xp,i}(t)$ at source location $\mathbf{r}_s$.

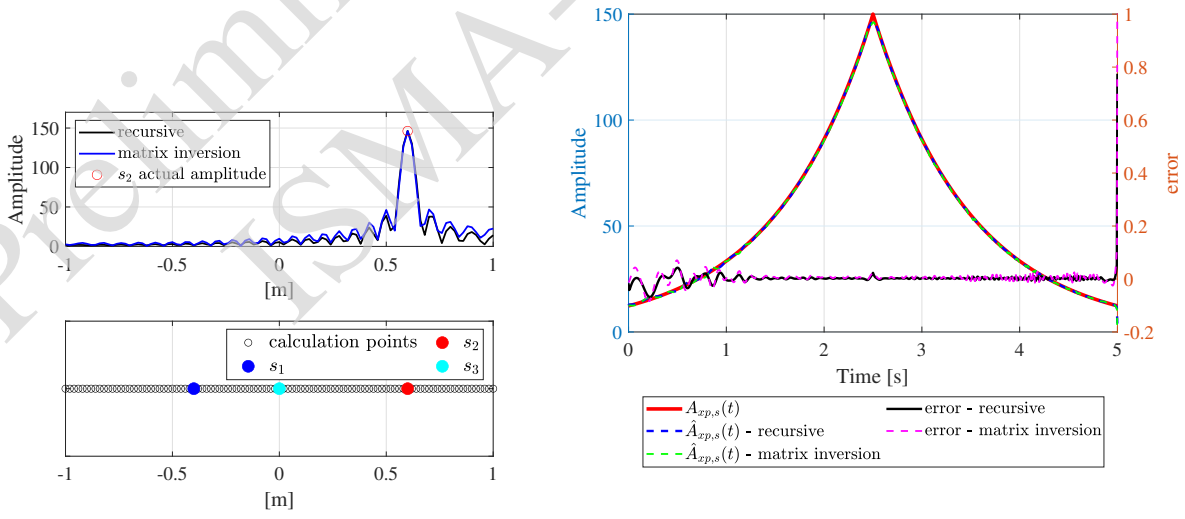

(a) (b)

Figure 3: Solution with OBBF for order 24.85: (a) source map at $f_p(t) = 2615$ Hz and (b) reconstructed envelop $\hat{A}_{xp,s}(t)$ of order 24.85 with recursive and matrix inversion OBBF; reconstruction error for both algorithms.

Figure 3a shows the source map at 2615 Hz associated with the order 24.85, which represents the presence of

single source s_2 and perfectly agrees with designed simulation model (Table 1). The recovered envelops at source location from the two algorithms are presented in Fig. 3b, with error calculated from absolute values as $\left(A_{xp,s}(t) - \hat{A}_{xp,s}(t)\right) / A_{xp,s}(t)$. Both the recursive and matrix inversion schemes of 1^{st} order expansion sufficiently retrieved the source envelop with negligible error. The start up transients at the envelop edge are due to the use of Savitzky–Golay lowpass filter during order-tracking. Also Fig. 3 showed that both the schemes functioned equivalent to each other while performing OBBF.

Comparing CBF (Fig. 2b) and OBBF (Fig. 3a) applied to the simulation model clearly showed OBBF improves tracking of order related sources and better quantifies when compared to CBF applied for non-stationary sources, especially at higher slew rates.

5 Industrial case study

To demonstrate the performances of OBBF on an industrial case, it is applied to an electric motor to localize the sound sources during a run-up. The results of OBBF reconstructed from recursive algorithm are compared to the Irregular Near-field Acoustic Holography (iNAH) sound power maps calculated from Simcenter Testlab software. The iNAH algorithm is based on acoustic holography and the spatial Fourier Transform of the observed sound field, and it can be used with an irregular microphone array.

5.1 Experimental set-up

An experimental investigation is conducted on a SimRod test rig at Siemens Industry Software NV, Leuven. A four pole induction motor is mounted on the test bed. The analysis discussed in this section is limited to the localization of sound sources on the top of the e-motor. A load value imposed by a second motor in the test rig controlled the required speed of the e-motor. At a distance of $0.3\,\mathrm{m}$ from top view, a planar Simcenter HD acoustic camera with 45 analogic microphones has been placed. A reference microphone is placed close to the emotor as shown in Fig. 4a. During the measurement, the signals were acquired by a front-end acquisition system LMS SCADAS.

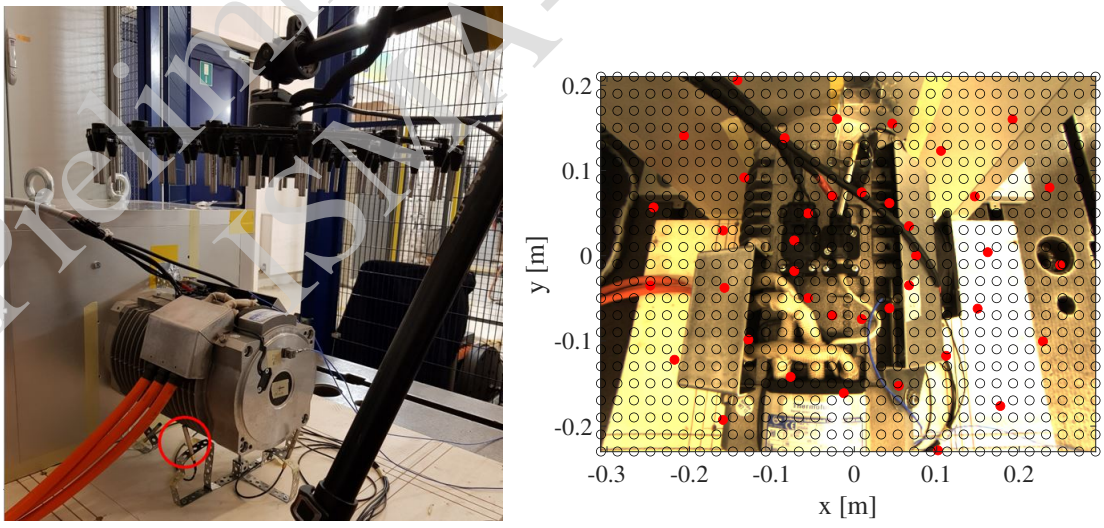

(a) (b)

Figure 4: Experimental set-up of electric motor in a non-anechoic environment: (a) e-motor mounted to a coupling unit; acoustic camera and a reference microphone (in red circle) and (b) scheme of 45 microphones (red dots) placed at the top of e-motor together with calculation points (black circles) spaced at 0.02 m.

5.2 OBBF validation

The study included a run up of high slew rate with linearly increasing reference speed from 0 rpm to 2450 rpm within a time span of $5.34\,\mathrm{s}$ with sampling frequency of $51\,200\,\mathrm{Hz}$. The observed signals were simultaneously recorded by the array microphones and then processed using order-based beamforming. As previously stated, the input to the OBBF is the order of interest extracted from order tracking of array microphones. The time-frequency map can be used to select the order of interest. However, the time-frequency map of array microphones has poor SNR, which might be due to non-anechoic environment, background noise, e-motor fan noise or radiation from other auxiliary systems on the test bed, making selection of order of interest difficult. As a result, the response from a reference microphone placed in the near-field of motor's housing is used in the selection of an interested order from its time-frequency map as shown in the Fig. 5a. Among several orders present in the system, one of the orders 79.5, excited by structural modes is chosen for performing order-based beamforming. The envelope of order 79.5 tracked by baseband demodulation order tracking in third-octave bands is shown in the Fig. 5b, which illustrates source localization around third octave band with central frequency $f_c = 2000\,\mathrm{Hz}$. The localization of sources on the electric motor is performed by the recursive order-based beamforming algorithm under free-field conditions.

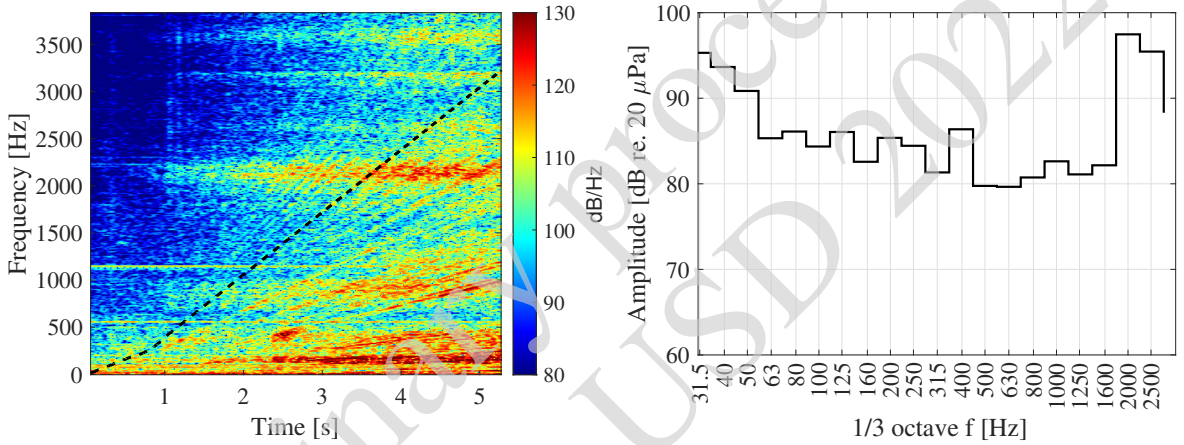

Figure 5: Order analysis of reference microphone signal: (a) Spectrogram with order 79.5 (- - -) highlighted and (b) Order 79.5 presented in third-octave band.

The output maps of recursive OBBF filtered in third-octave bands for $f_c = 1587\,\mathrm{Hz}, 2000\,\mathrm{Hz}$ and $2519\,\mathrm{Hz}$ are shown in the Fig. 6. For justification, the result is compared to the iNAH maps. A dynamic of $6\,\mathrm{dB}$ is maintained in both the OBBF and iNAH maps.

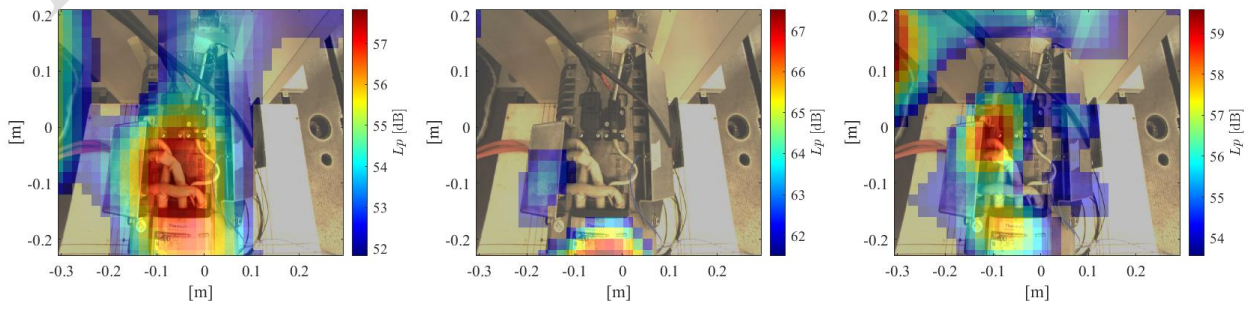

Figure 6: Third - octave recursive OBBF maps for order 79.5 with $dyn = 6\,\mathrm{dB}$: (a) 1414 Hz - 1781 Hz; (b) 1781 Hz - 2245 Hz and (c) 2245 Hz - 2828 Hz.

The observation from the preliminary validation shows that spatial localization of the radiating surface with OBBF is in good agreement with iNAH as shown in the Fig. 6 and Fig. 8. The sources tracked by OBBF have a better dynamic range, as shown in Fig. 6b and Fig. 8b, because the source characterized by iNAH includes smearing and bandwidth-time limitation, whereas in OBBF the sources are tracked along the orders without any affects. Moreover, Fig. 8b consists stronger side lobes when compared to Fig. 6b, due to the balance of energy caused by smearing in Fourier-based methods. This lends support to the proposed OBBF which aids improved tracking of orders. However, because free-field transfer functions were considered, the OBBF maps in the Fig. 6a and Fig. 6c contain artifacts that might be due to reflections from the reflective test bed, coupling unit or might be due to the non-anechoic environment.

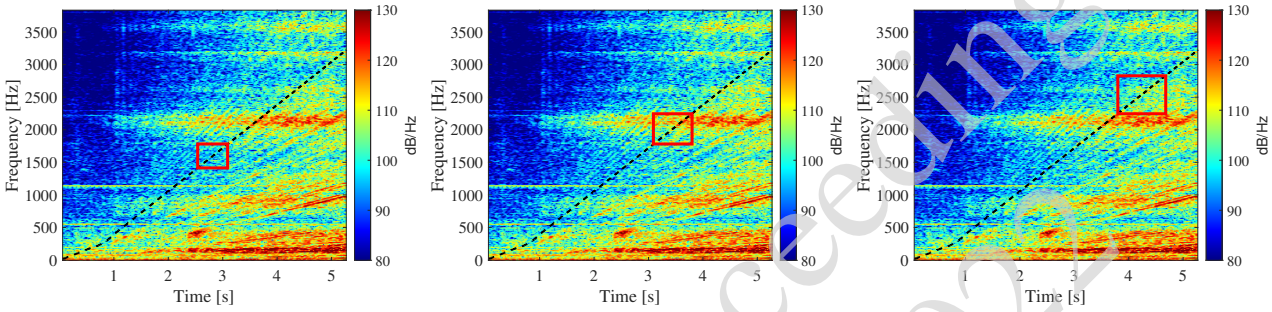

(a) (b) (c)

Figure 7: Time-frequency plot with selected third-octave band block (red rectangle) for calculating iNAH maps in Fig. 8; order 79.5 (- - -) highlighted: (a) 1414 Hz - 1781 Hz; (b) 1781 Hz - 2245 Hz and (c) 2245 Hz - 2828 Hz.

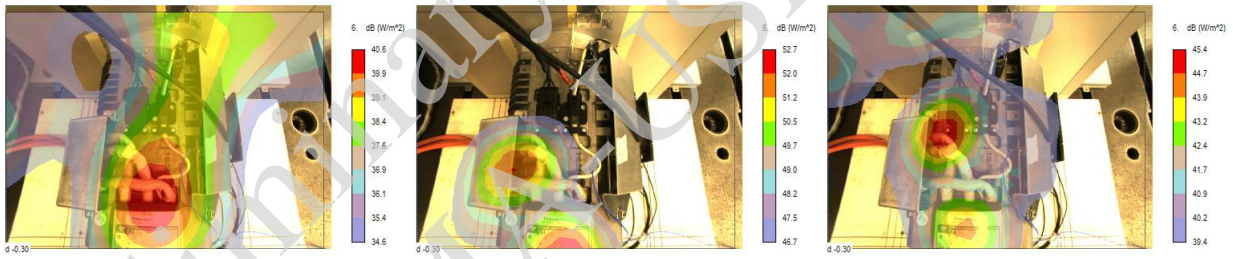

(a) (b) (c)

Figure 8: Third - octave iNAH maps with $dyn = 6\,\mathrm{dB}$: (a) 1414 Hz - 1781 Hz; (b) 1781 Hz - 2245 Hz and (c) 2245 Hz - 2828 Hz.

6 Conclusions

The paper proposed order-based beamforming, a novel technique for localizing non-stationary tonal sound sources during a rotating machinery's run-up / run-down operating modes. It has been shown that OBBF avoids smearing effect, bandwidth-time limitations that are present in conventional beamforming, while improving the tracking of order envelops. In addition, it provides the user with abundant information at every sample that can be attributed to source localization map at each instantaneous frequency. Although the current paper discusses OBBF considering free-field, it can be expanded to a complex field where the impulse response has a measurable support. To solve OBBF, recursive and matrix inversion algorithms are devised. Numerical simulations showed that the proposed algorithms adequately localized and quantified non-stationary sources even at higher slew rates and, in particular, in systems with close orders without smearing. The matrix inversion demands global propagation time to be chosen for each calculation point on the source grid to demodulate advanced signal, whereas in the recursive formulation, global propagation time

can be fixed for all calculation points making it simple, user friendly and computationally light. Nonetheless, due to the presence of a finite difference scheme, recursive formulation may be affected by time sampling, which can be reduced by appropriately selecting the optimal sampling frequency. For an advanced acoustic imaging, that takes into account for the source correlation, the matrix inversion formulation that structurally resembles inverse methods of frequency domain, can be expanded into a inverse methods of order domain. And, OBBF was found to be experimentally effective in a preliminary validation on an industrial case.

Acknowledgements

The authors would like to thank Siemens Industry Software NV, Belgium for providing the experimental database. We gratefully acknowledge the European Commission for its support of the Marie Sklodowska Curie program through the ETN ECO DRIVE project (GA 858018).

References

[1] L. Fritschi, A. L. Brown, R. Kim, D. Schwela, and S. Kephalopoulos, *Burden of disease from environmental noise: Quantification of healthy life years lost in Europe*, first edition ed. Copenhagen (Denmark): WHO Regional Office for Europe, 2011.

[2] European Environment Agency., *Environmental noise in Europe, 2020.*, 2020.

[3] G. M. Goetchius, "Leading the charge -the future of electric vehicle noise control," *Sound and Vibration*, vol. 45, pp. 5–8, 2011.

[4] Jason R. Blough, "Understanding Order Tracking Algorithm Limitations," May 2009, pp. 2009–01–2157. [Online]. Available: https://www.sae.org/content/2009-01-2157/

[5] J. Tuma, *Vehicle Gearbox Noise and Vibration : Measurement, Signal Analysis, Signal Processing and Noise Reduction Measures*. John Wiley & Sons, Incorporated, 2014.

[6] K. Fyfe and E. Munck, "Analysis of computed order tracking," *Mechanical Systems and Signal Processing*, vol. 11, no. 2, pp. 187–205, 1997.

[7] H. Vold and J. Leuridan, "High Resolution Order Tracking at Extreme Slew Rates, Using Kalman Tracking Filters," May 1993, p. 931288. [Online]. Available: https://www.sae.org/content/931288/

[8] J. G. Proakis and M. Salehi, *Communication systems engineering*. Prentice Hall, 2002.

[9] B. Fenyvesi, K. Tokaji, and C. Horváth, "Investigation of a pylons effect on the character of counter-rotating open rotor noise using beamforming technology," *Acta Acustica united with Acustica*, vol. 105, pp. 56–65, 01 2019.

[10] Q. Leclère, A. Pereira, C. Bailly, J. Antoni, and C. Picard, "A unified formalism for acoustic imaging based on microphone array measurements," *International Journal of Aeroacoustics*, vol. 16, no. 4-5, pp. 431–456, 2017.

[11] M.-C. Pan and Y.-F. Lin, "Further exploration of Vold–Kalman-filtering order tracking with shaft-speed information—I: Theoretical part, numerical implementation and parameter investigations," *Mechanical Systems and Signal Processing*, vol. 20, no. 5, pp. 1134–1154, Jul. 2006.

[12] M.-C. Pan and Y.-F. Lin, "Further exploration of Vold–Kalman-filtering order tracking with shaft-speed information—II: Engineering applications," *Mechanical Systems and Signal Processing*, vol. 20, no. 6, pp. 1410–1428, 2006, special Issue: Laser Doppler Vibrometry.

[13] J. Hald, "Use of non-stationary stsf for analysis of transient engine noise radiation," in *INTERNOISE*, vol. 3. New Zealand Acoustical Society; 1998, 1999, pp. 1439–1444.

[14] S. Paillasseur, J.-H. Thomas, and J.-C. Pascal, "Regularization for improving the deconvolution in real-time near-field acoustic holography," *The Journal of the Acoustical Society of America*, vol. 129, no. 6, pp. 3777–3787, 2011.

[15] M. R. Bai and J.-H. Lin, "Source identification system based on the time-domain nearfield equivalence source imaging: Fundamental theory and implementation," *Journal of Sound and Vibration*, vol. 307, no. 1, pp. 202–225, 2007.

[16] B. Lafon, M. Sidahmed, and L. Polac, "The concept of cyclic sound intensity and its application to acoustical imaging," *Journal of Sound and Vibration*, vol. 330, pp. 2107–2121, 04 2011.

[17] P. Shah, H. Vold, D. Hensley, E. Envia, and D. Stephens, "A high-resolution, continuous-scan acoustic measurement method for turbofan engine applications," *Journal of Turbomachinery*, vol. 137, 08 2015.

[18] P. N. Shah, A. White, D. Hensley, D. Papamoschou, and H. Vold, "Continuous-Scan Phased Array Measurement Methods for Turbofan Engine Acoustic Testing," *Journal of Engineering for Gas Turbines and Power*, vol. 141, no. 8, 02 2019, 081201. [Online]. Available: https://doi.org/10.1115/1.4042395

[19] C. Horváth, "Beamforming investigation of dominant counter-rotating open rotor tonal and broadband noise sources." *AIAA Journal*, vol. 53, no. 6, p. 1602, 2015.

[20] C. Horváth, E. Envia, and G. G. Podboy, "Limitations of phased array beamforming in open rotor noise source imaging." *AIAA Journal*, vol. 52, no. 8, pp. 1810 – 1817, 2014.

[21] B. Fenyvesi, J. Kriegseis, and C. Horváth, "Application of a combined method for the investigation of turbomachinery noise sources: Beamforming and proper orthogonal decomposition," 05 2019.

[22] T. Le Magueresse, A. Outrequin, M. Thivant, J.-L. Jouvray, and E. Robert, "3D acoustical characterization of an electrical motor by Bayesian Focusing," 03 2020.

[23] R. Cousson, Q. Leclère, M.-A. Pallas, and M. Berengier, "A time domain clean approach for the identification of acoustic moving sources," *Journal of Sound and Vibration*, vol. 443, 03 2019.

[24] S. Oerlemans, "Detection of aeroacoustic sound sources on aircraft and wind turbines," *Physical Review Letters*, 01 2009.

Appendix

A Nomenclature

M	Total number of microphones in the array
m	Index of microphone
I	Total number of calculation points on the source grid
i	Index of the calculation point
c_0	Speed of sound
$\mathbf{r}_s$	Position of the source
$\mathbf{r}_i$	Position of the calculation point
t	Time variable
f_s	Sampling frequency
T	Recording time length
N	Total number of samples
p	Order number
$\mathcal{P}$	A discrete set of orders
$x_s(t)$	Emitted source signal from a point source at $\mathbf{r}_s$
$y_m(t)$	Response signal at microphone m
$x_{p,s}(t)$	Mono-component signal of order p emitted from a point source at $\mathbf{r}_s$
$y_{p,m}(t)$	Pressure recorded by microphone m produced by $x_{p,s}(t)$
$\hat{A}_{xp,i}(t)$	Recovered envelop of a signal of order p at calculation point $\mathbf{r}_i$
$A_{yp,m}(t)$	Microphone envelop of a signal of order p at microphone m
$f(t)$	Instantaneous frequency
$\theta(t)$	Instantaneous phase of reference
$H(f)$	Transfer function at frequency f
$g(t)$	Impulse response of a low-pass filter
$\hat{X}_i(t, f)$	Beamforming output at calculation point i